Sixth International Symposium on Turbulence and Shear Flow Phenomena
Seoul, Korea, 22-24 June 2009

SECONDARY FLOW STRUCTURE OF TURBULENT COUETTE-POISEUILLE AND COUETTE FLOWS INSIDE A SQUARE DUCT FLOWS

H. W. Hsu, J. B. Hsu, W. Lo and C. A. Lin
Department of Power Mechanical Engineering, National Tsing Hua University,
Hsinchu 30013,TAIWAN
e-mail: calin@pme.nthu.edu.tw
Fax:+886-3-5722840

ABSTRACT

Turbulent Couette-Poiseuille and Couette flows inside a square duct at bulk Reynolds number 10,000 are investigated by the Large Eddy Simulations. Mean secondary flow is observed to be modified by the presence of moving wall where the symmetric vortex pattern vanishes. Secondary flow near the top corner shows a gradual change of vortex size and position as the moving wall velocity increased. It is interesting to note that a linear relation exits between the angle and the parameter $r = \frac{W_w}{W_{Bulk}}$, and a change in slope occurs at $r \sim 1.2$. Near the moving wall due to the reduction of the streamwise velocity fluctuation at the moving wall, turbulence structure gradually moves towards a rod-like axi-symmetric turbulence as r increases. As the wall velocity increases further for $r > 1.2$, the rod like structure disappears, and turbulence reverts to the disk like structure.

INTRODUCTION

Turbulent Couette-Poiseuille and Couette flows inside a square or rectangular cross-sectional duct are of considerable engineering interest because of their relevance to the compact heat exchangers and gas turbine cooling systems. The most studied flow is the turbulent Poiseuille flow inside a square duct and is characterized by existence of the secondary flow of Prandtl's second kind, which is not observed in circular ducts nor in laminar rectangular ducts. The secondary flow was observed to consist of a counter-rotating vortex pair symmetrically placed around the bisector of each corner. Although weak in magnitude (only a few percent of the streamwise bulk velocity), secondary flow is found to be very significant on the momentum and heat transfer and is often utilized as an enhancement of particle transport or heat transfer in different industrial devices.

There are also investigations directed to explore the influences of boundary wall geometry, non-isothermal effect, free surface and system rotation on the secondary flow pattern within turbulent Poiseuille duct flows (Vazquez and Metais, 2002; Pallares and Davidson, 2002, Brogolia et al., 2003). The above investigations have implied that with careful manipulation, the secondary flow is very much promising on enhancement of particle transport or heat transfer in different industrial devices. Also, the turbulence anisotropy in non-circular ducts could be modified by bounding wall geometry, heating, free surface and system rotation. Previous studies on turbulent Couette-Poiseuille flows have been conducted on simple plane channels. Thurlow and Klewicki (2000) found negative production of streamwise turbulence near the forward moving wall. Kuroda et al. (1993), Hwang and Lin (1998, 2003) identified different turbulence statistics and structures between the stationary and moving wall. However, little is known about the effect of moving wall on the turbulence anisotrpy and hence the resulting secondary flow within duct flows. Lo and Lin (2006a,2006b) found that the secondary flow structure correlates with the ratio of the speed of the moving wall and duct bulk flow, albeit the ratio was less than 1.17. It is not clear how the secondary flow behaves as the ratio increases.

In the present study, the assessment to this question is investigated by simulating the turbulent Couette-Poiseuille and Couette flows in a square duct based on large eddy simulation. Focus will be on the alternations of the secondary flow pattern within the duct and hence its turbulence structure due to the elevations of the ratio of moving wall velocity and duct bulk velocity.

MATHEMATICAL FORMULATIONS

Governing Equation and modeling.

The governing equations are grid-filtered, incompressible continuity and Navier-Stokes equations. In the present study, the Smagorinsky model (Smagorinsky, 1963) and dynamic model (Gemano et al., 1991) are adopted to model the sub-grid stress (SGS)

$$\tau^a = \tau^s_{ij} - \frac{\delta_{ij}}{3}\tau^s_{kk} = -2\rho(C_s\bar{\Delta})^2|\overline{S}|\overline{S}_{ij} \tag{1}$$

$$\tau^a = \tau^s_{ij} - \frac{\delta_{ij}}{3}\tau^s_{kk} = -2C_D\overline{\Delta}^2|\overline{S}|\overline{S}_{ij} \tag{2}$$

where $C_s = 0.1$, δ_{ij} is the Krinecker delta, $S_{ij} = \frac{\partial \overline{u}_i}{\partial x_j} + \frac{\partial \overline{u}_j}{\partial x_i}$, and, Δ defined as $(\Delta x \Delta y \Delta z)^{1/3}$ is the length scale. It can be seen that the mesh size is used as the filtering operator. For Smagorinsky, A Van Driest damping function accounts for the effect of the wall on sub-grid scales is adopted here and takes the form as, $l_m = \kappa y[1 - exp(-\frac{y^+}{25})]$.

For dynamic model, the model coefficient C_D is allowed to be a function of space and time. Following Lilly (1992), the coefficient is obtained using the least square approach, i.e.

$$C_D = -\frac{1}{2}\frac{\langle L_{ij}M_{ij}\rangle}{\langle M_{ij}M_{ij}\rangle} \tag{3}$$

$$L_{ij} - \frac{\delta_{ij}}{3}L_{kk} = -2C_D M_{ij} \tag{4}$$

$$M_{ij} = \widehat{\overline{\Delta}}^2\,\widehat{|\overline{S}|}\widehat{\overline{S}}_{ij} - \Delta^2\widehat{|\overline{S}|\overline{S}_{ij}} \tag{5}$$

where the brackets $\langle\rangle$ denote an average over the homogeneous directions for the numerator and denominator. They are assumed to be functions of the inhomogeneous direction and time only.

Numerical and parallel Algorithms.

A semi-implicit, fractional step method proposed by Kim and Moin (1985) and the finite volume method are employed to solve the filtered incompressible Navier-Stokes equations. Spatial derivatives are approximated using second-order central difference schemes. The non-linear terms are advanced with the Adams-Bashfoth scheme in time, whereas the Crank-Nicholson scheme is adopted for the diffusion terms. The discretized algebraic equations from momentum equations are solved by the preconditioned Conjugate Gradient solver. In each time step a Poisson equation is solved to obtain a divergence free velocity field. Because the grid spacing is uniform in the streamwise direction, together with the adoption of the periodic boundary conditions, Fourier transform can be used to reduce the 3-D Poisson equation to uncoupled 2-D algebraic equations. The algebraic equations are solved by the direct solver using LU decomposition.

The computational domain consists of $D \times D \times 2\pi D$ (D is the width of the duct) in the horizontal (x), vertical (y) and streamwise (z) directions, respectively. Here, u, v and w are used to denote, respectively, the velocity components in the horizontal, vertical, and streamwise directions. No-slip boundary conditions for the velocity components are applied at the four bounding walls and periodic boundary condition is employed in the steramwise direction at the inlet and outlet of the square duct. Top wall (y=D) is either stationary or moving in the positive streamwise direction, while other bounding walls are at rest. In all the cases considered here the grid sizes employed are (128x128x96) and (128x128x128), respectively for Smargorinsky and dynamic models in spanwise, normal, and streamwise directions. Grid is symmetrically clustered using hyperbolic tangent functions towards the walls on the cross-plane of the duct with minimum and maximum spacing of $\triangle x^+, \triangle y^+$ approximately as 1.2 and 7.8. In the streamwise direction, the grid is uniformly distributed with $\triangle z^+ \sim 35 - 40$.

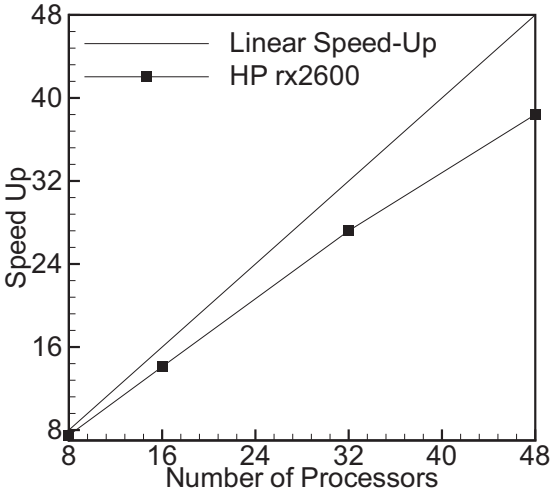

Figure 1: Parallel performance of present simulation.

In the present parallel implementation, the single program multiple data (SPMD) environment is adopted. The domain decomposition is done on the last dimension of the three dimensional computation domain due to the explicit numerical treatment on that direction. The simulation is conducted on the HP Integrity rx2600 server (192 Nodes) with about 80 percent efficiency when 48 CPUs are employed[?]. Linear speed-up is not reached in present parallel implementation mainly due to the global data movement required by the Fast Fourier Transform in the homogenous direction.

Table 1: Table I: Flow conditions of simulated cases adopting Smagorinsky model; Re_τ is defined by the mean friction velocity averaged over four solid walls (t=top,b=bottom wall); W_w denotes the velocity of the moving wall and W_{Bulk} is the bulk velocity; $Re_c = \frac{W_w D}{\nu}$; $r = \frac{W_w}{W_{Bulk}}$.

128x128x96	$Re_{\tau t}$	$Re_{\tau b}$	Re_{Bulk}	Re_c	r
Case P	604	604	10000	0	0
Case CP1	441	586	10000	6000	0.6
Case CP2	332	581	10000	9136	0.91
Case CP3	317	574	10000	11420	1.14
Case CP4	387	570	10000	13704	1.37
Case CP5	480	563	10000	15998	1.60
Case CP6	654	551	10000	20556	2.06
Case CP7	744	544	10000	22840	2.28
Case CP8	919	526	10000	27408	2.74
Case C	1167	512	10247	34260	3.34
Kuroda et al.	35	308	5178	6000	1.16

Table 2: Table II: Flow conditions of simulated cases using the Dynamic Smagorinsky model

128x128x128	$Re_{\tau t}$	$Re_{\tau b}$	Re_{Bulk}	Re_c	r
Case P	636	636	10000	0	0
Case CP1	422	612	10000	6000	0.6
Case CP3	324	595	10000	11420	1.14
Case CP5	493	580	10000	15998	1.60
Case CP7	744	544	10000	22840	2.28
Kuroda et al.	35	308	5178	6000	1.16

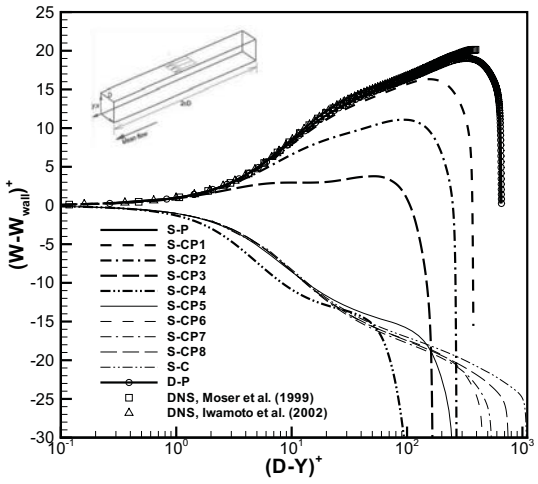

Figure 2: Mean streamwise velocity along the wall bisector for case P to C.

RESULTS

Schematic picture of the flows simulated is shown in Figure 2. Here, fully developed, incompressible turbulent flows

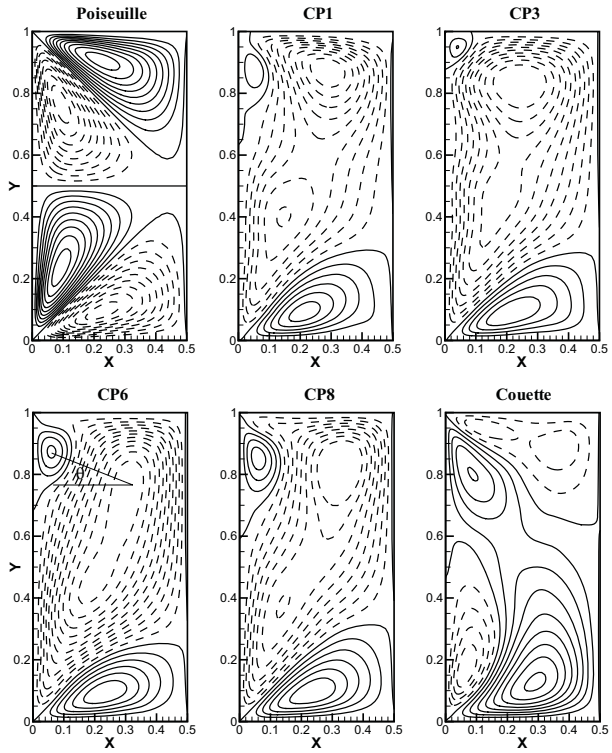

Figure 3: Streamlines of mean secondary flow for case P to C; solid lines for counter-clockwise rotation, dashed lines for clockwise rotation.

inside a square duct are considered, where the basic parameters are summarized in Tables I and II. Reynolds number is kept at 10000 except for Couette flow and the importance of Couette strain rate in this combined flow field can be indicated by the ratio $r = W_w/W_{bulk}$. To maintain the constant bulk Reynolds number, the driving pressure gradient is modified at each time step by the bulk Reynolds number.

Mean secondary flow structure.

Mean streamwise velocity distributions from top wall along the wall bisector, ie. x/D=0.5, at different mean Couette strain rates are shown in Figure 2. For Case P and Case CP1, the velocity distributions follow closely the 2D channel flow DNS data of Moser et al. (1999)(Ret:395) and Iwomoto et al.(2002) (Ret:300). However, at higher Couette velocity due to the reduction of shear rate, departures from the logarithmic distributions are observed for cases CP2-C, which are consistent with the findings of plane Couette-Poiseuille flow of Kuroda et al. (1993). It should be noted that for all cases considered logarithmic distributions prevail at the bottom wall, except in the vicinity of side wall.

Streamlines of mean secondary flow for cases P to C are shown in Figure 3. Due to the symmetrical nature of the flow, only half the domain is shown here for simplicity. The vortex structure is clearly visible, where solid and dashed lines represent the counter-clockwise and clockwise vortices, respectively. The presence of the moving wall does influence the patterns of the secondary flow, where the two clockwise rotating vortices gradually merge in tandem with Couette velocity. The angle formed by the horizontal x axis and the line joining the two vortex cores becomes a good representation of the relative vortex positions. This angle is calculated and plotted against the parameter r defined by $r = (W_w/W_{Bulk})$. It is interesting to note that a linear relation exits between the angle and the parameter r, as shown in Figure 4, and a change in slope occurs at $r \sim 1.2$. Both the Smagorinsky model (SM) and the dynamic Smargorinsky model (DSM) show similar trend.

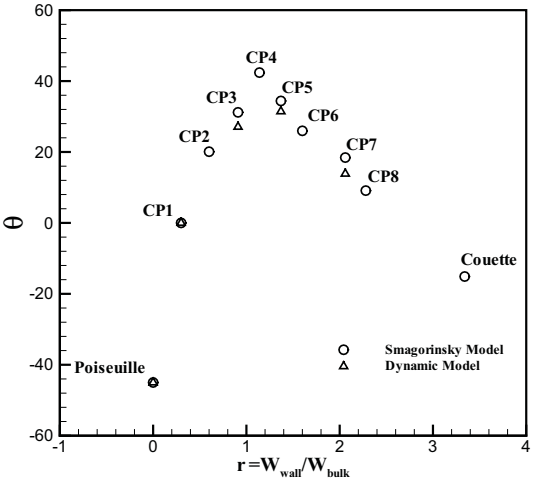

Figure 4: Angles between vortex cores near the top corners.

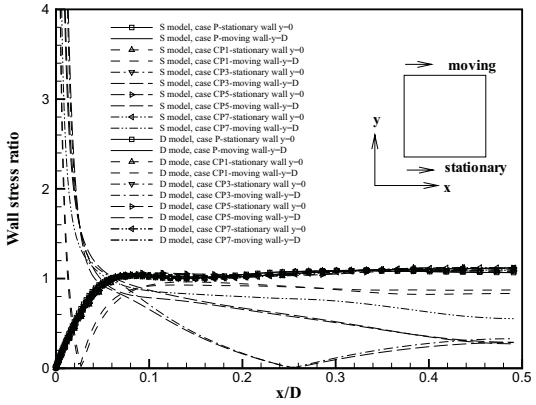

Figure 5: Wall stress variation-cases P-CP4.

Local wall stress($\tau_w/\overline{\tau_w}$) distributions along the top moving and bottom stationary walls are shown in figs. 5 to 7, where Fig. 5 show the comparisons of predicted wall stress using SM and DSM. Both the SM and DSM predict similar wall stress distributions, shown in Fig. 5, indicating that at this grid density the influence of the sub-grid stress modelling is not influential. Thus further computations will adopt SM approach. By reference to Figs. 6 and 7, the distributions at the stationary wall follow that of a turbulent Poiseuille flow and is good agreement with DNS data of Huser et al.(1993) The wall stresses along the moving wall show dramatic different profiles, especially near the top corner. Here, high shear stress is generated by the fast moving wall and the nearby stagnant fluid. The zero wall stress location, which roughly coincide with the zero $\partial W/\partial y$ region, moves towards the central region as the wall velocity increases. As the moving wall velocity increases further, the wall stress distributions approach their bottom wall counterpart.

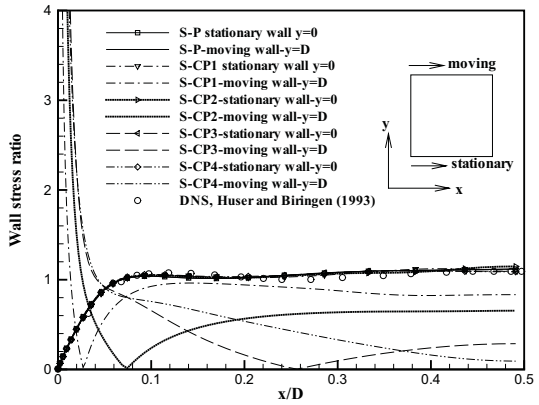

Figure 6: Wall stress variation-cases P-CP4.

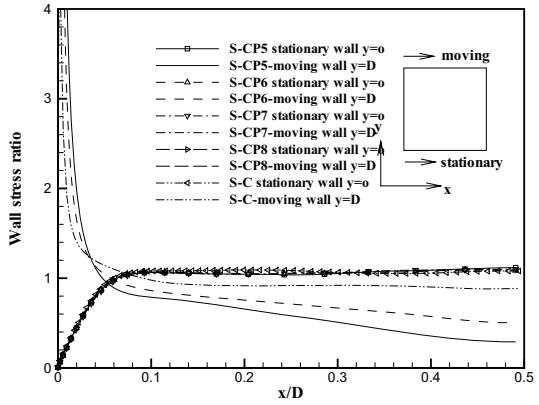

Figure 7: Wall stress variation-cases CP5-C

Figure 8 show the cross-plane distribution of the resolved turbulence kinetic energy. In the Poiseuille flow the distribution shows locally maximum near the stationary wall. For the Couette-Poiseuille flows, near the moving wall, turbulence kinetic energy is first damped near the moving wall, which is caused by the reduced mean shear at this region. The decrease in turbulence kinetic energy is more evident near the wall-bisector (x/D=0.5) than near the side wall. As the moving wall velocity increases, the distribution of the maximum turbulence kinetic energy is gradually moved from the side stationary wall to the top corner, and then migrates to the top wall. However, near the bottom stationary wall, the distributions of the kinetic energy are not influenced by the top moving wall. As for Couette flow, the kinetic energy distribution is similar to the Coueete-Poiseuille flows at high level of r.

Detailed examinations of the turbulence quantities can be seen in Figures 9 and 10, showing the predicted turbulence production and kinetic energy distributions along the wall bisector at x/D=0.5. Here, the DNS data of plane channel flow (Iwamoto et al., 2002) is included for comparisons. By reference to Figures 9 (a)-(b), it is clearly observed that the turbulence level near the stationary wall remains unchanged. However, near the moving wall, it is decreased first in tandem with the increase of the moving wall velocity. However, beyond $r > 1.2$, kinetic energy gradually increases as Couette velocity increases further. The levels of the ki-

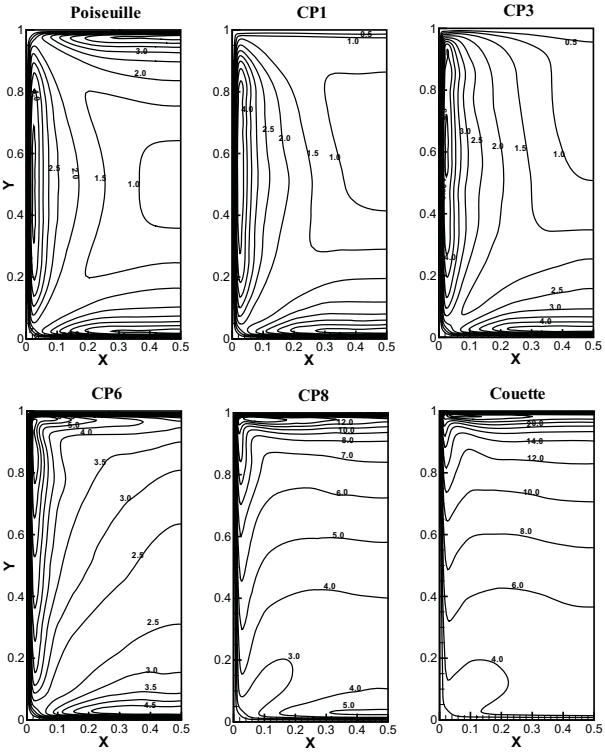

Figure 8: Turbulence kinetic energy for case P to C.

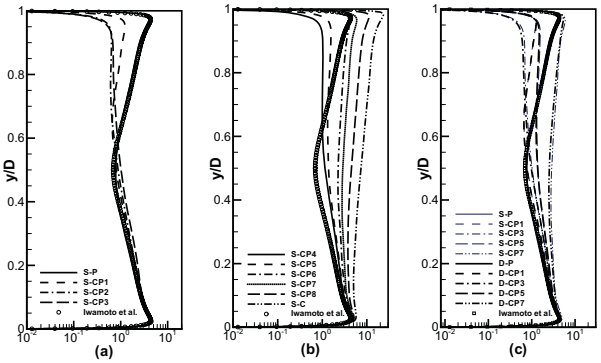

Figure 9: (a)-(b)Turbulence kinetic energy for SM: case P to Co. (c)Turbulence kinetic energy for SM and DSM.

netic energy correlate well with the production terms shown in Figs. 10 (a)-(b). It is also interesting to note that the low level of kinetic energy production gradually moves away from the centre core and towards the moving wall. Comparisons of the predicted kinetic energy levels and the production rates are shown in Figs. 9 (c) and 10 (c). Similar distributions are obtained, which indicates again the sub-grid stress modelling is not influential here.

Anisotropy invariant map.

The anisotropy invariant map (AIM) is introduced here in order to provide more specific description of the turbulence structures. It was demonstrated that the mean and turbulence fields are modified by the Couette wall. The invariant functions provide more specific description of tur-

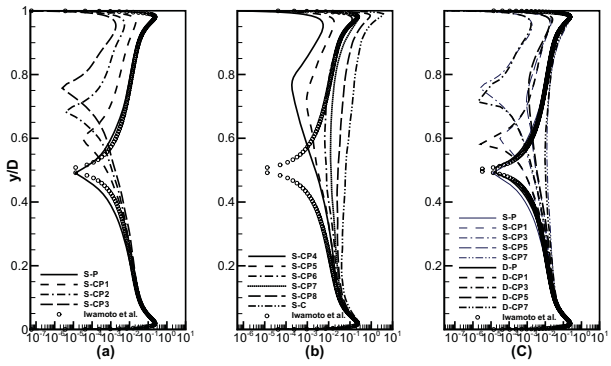

Figure 10: (a)-(b)Turbulence production kinetic energy for SM: case P to Co. (c)Turbulence production kinetic energy for SM and DSM.

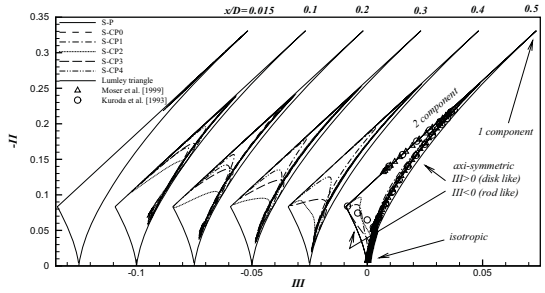

Figure 11: Anisotropy invariant map at x/D=0.5 for case P to CP4.

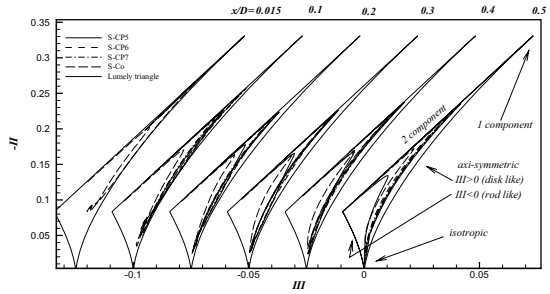

Figure 12: Anisotropy invariant map at x/D=0.5 for case CP5 to C.

bulence structure and hence anisotropy. The invariants of the Reynolds stress tensors are defined as $II = -(1/2)b_{ij}b_{ji}$, $III = (1/3)b_{ij}b_{jk}b_{ki}$ and $b_{ij} =< u_i'u_j' > / < u_k'u_k' > -1/3\delta_{ij}$. A cross-plot of -II versus III forms the anisotropy invariant map (AIM). All realizable Reynolds stress invariants must lie within the Lumley triangle (Lumley, 1978). This region is bounded by three lines, namely two component state, $-II = 3(III + 1/27)$, and two axi-symmetric states, $III = \pm(-II/3)^{3/2}$. For the axi-symmetric states, Lee and Reynolds (1985) described the positive and negative III as disk-like and rod-like turbulence, respectively. The intersections of the bounding lines represent the isotropic, one-component and two-component axi-symmetric states of turbulence.

The anisotropy invariant maps at several horizonal locations are presented in Figs. 11 and 12. Here, DNS data of plane channel flow (Moser et al., 1999) and plane Couette-Poiseuille flow (Kuroda et al., 1993) are also included for comparison. Near the stationary wall ($y/D \leq 0.5$), turbulence behaviors of different Couette-Poiseuille flows resemble those of the Poiseuille flow. In particular, the turbulence structure is similar to the plane channel flow, where turbulence approaches two-component state near the stationary wall due to the highly suppressed wall-normal velocity fluctuation. It moves toward the one-component state till $y^+ \sim 8$ (Antonia et al., 1977; Salinas-Vázquez and Métais, 2005) and then follows the positive III axi-symmetric branch (disk-like turbulence, Lee and Reynolds, 1985) to the isotropic state at the duct center. However, near the moving wall due to the reduction of the streamwise velocity fluctuation at the moving wall, turbulence structure gradually moves towards a rod-like axi-symmetric turbulence (negative III) as r increases. As the wall velocity increases further for $r > 1.2$, the rod like structure disappears, and turbulence reverts to the disk like structure, as is shown in Fig. 12.

CONCLUSIONS

The turbulent Couette-Poiseuille and Couette flows inside a square duct are investigated by present simulation procedures. Mean secondary flow is observed to be modified by the presence of moving wall where the symmetric vortex pattern vanishes. Secondary flow near the top corner shows a gradual change of vortex size and position as the moving wall velocity increased. The vortex pair consists of a dominate (clock-wise) and relatively smaller (counter-clockwise) vortex. It is interesting to note that a linear relation exits between the angle and the parameter r, and a change in slope occurs at $r \sim$1.2. Near the moving wall due to the reduction of the streamwise velocity fluctuation at the moving wall, turbulence structure gradually moves towards a rod-like axi-symmetric turbulence (negative III) as r increases. As the wall velocity increases further for $r > 1.2$, the rod like structure disappears, and turbulence reverts to the disk like structure.

ACKNOWLEDGMENTS

This research work is supported by the National Science Council of Taiwan under grant 95-2221-E-007 -227 and the computational facilities are provided by the National Center for High-Performance Computing of Taiwan which the authors gratefully acknowledge.

REFERENCES

Antonia, R. A., Danh, H. Q. and Prabhu, A., 1977, "Response of turbulent boundary layer to a step change of heat flux," *J. Fluid Mech.*, Vol. 99, pp. 153-177.

Brogolia, R., Pascarelli, A., and Piomelli, U., 2003, "Large eddy simulations of ducts with a free surface," *J. Fluid Mech.*, vol. 484, pp.223-253.

Germano, M. and Piomelli, U., Moin, P. and Cabot, W. H., 1991, "A dynamic subgrid-scale eddy viscosity model," *physics of Fluids A*, Vol. 3, No. 7, pp. 1760-1765.

Huser, A. and Biringen, S., 1993, "Direct numerical simulation of turbulent flow in a square duct," *J. Fluid Mech.*, vol. 257, pp.65-95.

Hwang, C. B. and Lin, C. A., 1998, "Improved low-reynolds -number k- model based on direct numerical simulation data," *AIAA J.*, vol. 36, pp. 38-43.

Hwang, C. B. and Lin, C. A., 2003 "Low-reynolds-number k- modeling of nonstationary solid boundary flows," *AIAA J.*, vol. 41, pp. 168-175.

Iwamoto, K., Suzuki, Y. and Kasagi, N., 2002, "Reynolds number effect on wall turbulence: toward effective feedback control," *International J. of Heat and Fluid Flow Mech.*, Vol. 484, pp. 223-253.

Kim, J. and Moin, P., 1985 "Application of a fractional-step method to incompressible Navier-Stokes equations," *J. Comput. Phys.*, Vol. 59, Issue 2, 308-323.

Kim, J., Moin, P. and Moser, R., 1987,"Turbulence statistics in fully developed channel flow at low Reynolds number," *J. Fluid Mech.*, Vol. 177, pp. 133–166.

Kuroda, A., Kasagi, N. and Hirata, M., 1993, "Direct numerical simulation of turbulent plane CouetteVPoiseuille flows: Effect of mean shear rate on the near wall turbulence structures," *Proceeding of the 9th Symposium on Turbulent Shear Flow*, Kyoto, Japan, pp.8.4.1-8.4.6.

Lee, M. J. and Reynolds, W. C., 1985, "Numerical experiments on the structure of homogeneous turbulence," Report TF-24, Thermoscience Division, Stanford University.

Lilly, D. K., 1992, "A Proposed Modification of the Germano Subgrid-Scale Closure Method," *Physics of Fluids A*, Vol. 4, No. 3, pp. 633-635.

Lo, W. and Lin, C. A. 2006a, "Mean and turbulence structures of Couette-Poiseuille flows at different mean shear rates in a square duct," *Phys. Fluids* 18,068103.

Lo, W. and Lin, C. A. 2006b, "Prediction of secondary flow structure in turbulent Couette-Poiseuille flows inside a square duct," *PCFD 2006*.

Lumley, J. L., 1978, "Computational modeling of turbulent flows," Advances in Applied Mechanics, Vol. 18, pp. 123-176.

Moser, R., Kim, J. and Mansour, N., 1999, "Direct numerical simulation of turbulent channel flow up to Retau=590," *Phys. Fluids*, Vol. 11, pp. 943-945.

Pallares, J. and Davidson, L., 2002, "Large eddy simulations of turbulent heat transfer in stationary and rotating square ducts," *Phys. Fluids*, vol. 14, pp. 2804-2816.

Piomelli, U. and Liu, A., 1995, "Large eddy simulation of rotating channel flows using a localized dynamic midel" *Phys. Fluids*, Vol. 7, pp. 839-848.

Salinas Vazquez, M., Vicente Rodriguez, W. and Issa, R., 2005, "Effects of ridged walls on the heat transfer in a heated square duct," *Int. J. Heat and Mass Transfer*, Vol. 48, pp. 2050-2063.

Smagorinsky, J., 1963 "General circulation experiments with the primitive equations," I. The basic experiment. In Mon. Weather Rev., vol. 91 of 3, pp. 99-164.

Thurlow, E. M. and Klewicki, J. C., 2000, "Experimental study of turbulent poiseuille-couette flow," *Phys. Fluids*, vol. 4, pp. 865-875.